Two-dimensional filtering in the Fourier domain of transient grating coherent artifacts in time-resolved spectroscopy

Marlo Vega, Jean-François Bryche, P.-L. Karsenti, Philippe Gogol, M. Canva, P.G. Charette

Two-dimensional filtering in the Fourier domain of transient grating coherent artifacts in time-resolved spectroscopy

M. Vega [1,2,3], J.-F. Bryche [1,3,4,*], P.-L. Karsenti [4], P. Gogol [1,3,5], M. Canva [1,3], P.G. Charette [1,3]

[1] *Laboratoire Nanotechnologies Nanosystèmes (LN2), CNRS, Université de Sherbrooke, Sherbrooke, QC, Canada*
[2] *Université Paris-Saclay, Institut d'Optique Graduate School, CNRS, Laboratoire Charles Fabry, Palaiseau, France*
[3] *Institut Interdisciplinaire d'Innovation Technologique (3IT), Université de Sherbrooke, Sherbrooke, QC, Canada*
[4] *Faculté des Sciences, Université de Sherbrooke, Sherbrooke, QC, Canada*
[5] *Centre de Nanosciences et de Nanotechnologies, Université Paris-Saclay, CNRS, Palaiseau, France*

HIGHLIGHTS

- Coherent artifacts in time resolved spectroscopy, such as transient grating artifacts, distort experimental measurements.
- Coherent artifact removal can be formulated as a two-dimensional nu-merical problem for greatly improved efficacy.
- Fourier domain filtering can remove artifact distortions without significantly altering the underlying baseline data. The proposed artifact filtering method is demonstrated on data from metal nanostructures and fluorophores in solution.
- The proposed method is applicable to other types of coherent artifacts in time and wavelength-resolved spectroscopy data.

Keywords:
Femtosecond time resolved spectroscopy; Pump-probe spectroscopy; Non-linear coherent artifact filtering Transient grating artifact; Fourier domain filtering

GRAPHICAL ABSTRACT

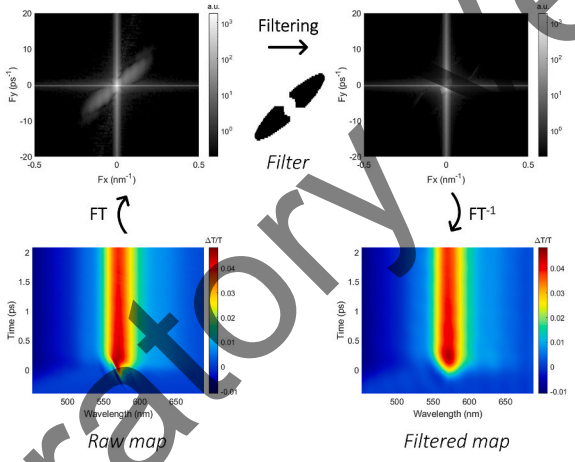

ABSTRACT

Removal of coherent artifacts is important in the analysis of time and wavelength resolved spectroscopy data. By taking advantage of the strong correlation between spectra acquired sequentially in time, artifact removal can be formulated as a 2D problem for improved effectiveness. This paper proposes a 2D method to remove transient grating coherent artifacts from femtosecond time-resolved spectroscopy data based on filtering in the Fourier domain, leading to better estimation of the material parameters from the measured data. The method is simple, intuitive, and light on computation resources. The effectiveness of the method is demonstrated with experimental data acquired from a bare gold film with and without coherent artifacts using mutually parallel and perpen-dicular pump/probe polarizations, as well as with more complex samples (nanostructured gold film on a glass substrate and rhodamine fluorophores in solution). The proposed method is expected to be applicable to coherent artifact removal in other types of time and wavelength-resolved spectroscopy data.

* Corresponding author. Laboratoire Nanotechnologies Nanosystèmes (LN2), CNRS, Université de Sherbrooke - Sherbrooke, QC, Canada.
E-mail address: jean-francois.bryche@cnrs.fr (J.-F. Bryche).

https://doi.org/10.1016/j.aca.2023.341820

Received 17 April 2023; Received in revised form 26 July 2023;

1. Introduction

Femtosecond time-resolved spectroscopy is a powerful method for measuring ultra-fast relaxation dynamics following pulsed photoexcitation. The method uses two short (fs) laser pulses: a first energetic pump pulse to excite the system and a delayed probe pulse to track the time evolution of pump-induced optical property changes via the transmission, reflection and/or absorption spectra. The high temporal resolution afforded by the short duration of the pulses [1,2] enables the study of physical phenomena such as electronic and vibrational molecule relaxation [3] and carrier lifetime [4], as well as thermal relaxation in metals [5]. However, non-linear interactions between the pump and probe pulses in the sample generate unwanted artifacts in the measured spectra [1,6–8]. These artifacts are termed "coherent" since they appear only when the pump and probe overlap in time. Coherent artifacts can arise from phenomena such as two-photon absorption [6,9], cross-phase modulation [6,10,11], stimulated Raman amplification [2,6], and transient grating effects [7,12–15]. In the latter case, when the pump and the probe overlap in time, wavelength and space, an interference pattern is generated in the sample, spatially modulating its refractive index in a grating fashion. This induced "transient grating" diffracts the pump pulse into the reflected (or transmitted) probe pulse, adding un-wanted components to the signal sampled by the detector [7], which can interfere with the estimation of the material parameters from the measured data.

These transient grating artifacts can be removed or, at least, minimized by experimental design, for example with perpendicular pump-probe polarization [7,8,13], by increasing the relative angle between the pump and probe [7], or by adjusting their relative intensities [13]. However, such solutions cannot be employed in many cases due to constraints arising from the nature of the sample or the phenomena under study (ex: molecules or nanoparticles sensitive to the orientation of the light polarization) and/or the experimental setup (ex: limited flexibility with pump-probe incidence angle, low signal-to-noise ratio when decreasing probe intensity). Alternatively, coherent artifacts (transient grating type or otherwise) can be removed by post-processing. In most cases, the removal of coherent artifacts is treated as a 1D problem where the time-delayed spectra are processed individually [16, 17]. However, by taking advantage of the strong correlation between successive spectra, coherent artifact removal can be formulated as a 2D problem for greatly improved filtering efficacy. For example, de Rooi et al. [18] proposed a method based on a mixture model where opti-mization is used to separate the 2D spectroscopy maps into a smooth baseline image and a second image containing the unwanted artifacts.

In this work, we propose a novel 2D method for transient grating artifact removal based on filtering time and wavelength resolved transient spectroscopy data in the Fourier domain. Transient grating artifacts have a very distinctive spectral signature in the Fourier domain that is reasonably well separated from the baseline information spectral content, with key characteristics directly related to experimental pa-rameters. Hence, such artifacts can be filtered effectively using fre-quency domain methods, making use of a priori information in the filter design. In both our proposed method and [18], some filtering parame-ters must be set by the user. In Ref. [18], two scale factors in a compound cost function used in the minimization must be specified. These pa-rameters have no direct physical analogue and must ideally be estimated from simulation data. In our case, two parameters for image thresh-olding must be specified. Because of the distinctive shape of the artifact spectral signature, the parameters are very intuitive to determine visu-ally from the spectrum.

The proposed method is described below and demonstrated with data acquired from a bare unstructured metal surface as well as with more complex samples (nanostructured gold film on a glass substrate and rhodamine fluorophores in solution). The paper describes the experimental setup used for acquiring transient reflectance/transmittance maps with either mutually parallel or perpendicular pump-probe polarizations, to generate data with and without artifacts, respectively. Though the method was developed for removing transient grating artifacts, it is applicable to other types of coherent artifacts, as discussed below.

2. Material and methods

2.1. Femtosecond time-resolved spectroscopy measurement system

Transient reflectance and transmittance maps were acquired with a Ti:sapphire oscillator and a regenerative amplifier (Solstice, Spectra-Physics) producing 150 fs FWHM light pulses at 1 kHz with a spectrum centered at 795 nm (15 nm FWHM). The laser source was coupled to an optical parametric amplifier (OPA 800CF, Spectra-Physics) to generate pump pulses from 300 nm to 3 μm. A small fraction of the laser source was focused on a sapphire window to generate a white light continuum probe by self-phase modulation. Pump pulses were delayed with respect to the probe using a linear translation stage yielding a resolution of 6.6 fs. One of every two pump pulses was blocked with a chopper for separate measurement of the reference transmitted/re-flected probes pulse from the pump-modified transmitted/reflected probe pulses. The pump and probe beams were focused on the sample using parabolic mirrors with beam waists of 75 μm and 35 μm at inci-dence angles of -8° and 6° relative to the surface normal, respectively. Transmitted and reflected probe spectra were sampled spatially using diffraction gratings and CCD cameras. The pump beam was polarized perpendicularly to the plane of incidence (plane containing the incident, reflected, and transmitted rays, forming an angle of 90° with the sample surface). The probe polarization could be either perpendicular or par-allel to the plane of incidence. Probe chirp was corrected following the procedure described in Ref. [2].

2.2. Samples: smooth metal film, nanostructured metal film, fluorophores in solution

Metal film samples were prepared by first depositing a 30 nm thickness Au film (2 nm Ti adhesion layer) on borosilicate glass (BK7) substrates. Smooth unstructured Au film samples were used as reference samples. The nanostructured Au film samples consisted of an array of asymmetric crosses (300/410 nm short/long arm length, 60 nm arm width, 60 nm film height) in an array (530/640 nm center-to-center period along the short/long arms) fabricated by e-beam lithography and lift-off atop the 30 nm Au film [19]. The fluorophore solution consisted of rhodamine 6G fluorophores diluted in ethanol and CS_2 (1:3) in a cuvette. We used CS2 solvent for its high χ^3 to maximize transient grating artifact intensity and added ethanol to dilute the solution as rhodamine 6G is not soluble in pure CS2.

3. Results and discussion

3.1. Description of the filtering method, characterization with a reference sample

Transient reflectance maps were acquired from a reference sample consisting of a smooth Au film. The maps were acquired using both mutually parallel and perpendicular pump-probe polarizations to generate data with and without transient grating artifacts. Fig. 1(a) and (b) show the time and wavelength resolved maps of normalized reflectance variation ($\Delta R/R$) for both cases, where R is the reference reflectance (without the pump) and ΔR is the reflectance variation induced by absorption of the pump pulse centered at 600 nm. Positive $\Delta R/R$ values around 500 nm and negative $\Delta R/R$ values from 540 nm onwards correspond to gold interband transitions [20].

As expected, the artifact due to the transient grating effect is present only for the case of mutually parallel pump/probe polarization as seen in Fig. 1(b), while Fig. 1(a) shows the "baseline" map without artifact (the

objective of the filtering process is to remove the artifact from a reflectance map to recover the baseline). The artifact is centered vertically at zero pump/probe time delay and horizontally at the pump center wavelength (600 nm). The extent of the edge-shaped artifact is determined by the spectral bandwidth ($\Delta\lambda \sim 28$ nm) and chirp of the pump ($\Delta t \sim 0.35$ ps), forming an angle of $\alpha = -\tan^{-1}(\Delta t/\Delta\lambda)$ with the horizontal. The downward orientation (negative slope) is due to the positive chirp of the pump (longer wavelengths lead shorter wavelengths in the pulses). The baseline signal levels in both maps are very close since reflectance from a gold film at shallow incidence angles is almost polarization independent.

Since the transient grating artifact has a sharp and roughly straight edge-like shape at a downward angle α in the reflectance maps, its spatial frequency content is expected to be concentrated away from the origin along a diagonal at an angle of $\Theta = \pi/2 + \alpha$ from the horizontal in the upper-right quadrant in 2D Fourier space (positive frequencies) with a reflection in the lower-left quadrant (negative frequencies). The rela-tively smooth (artifact-free) baseline information in the reflectance maps has a much lower spatial frequency content and is expected to be mainly clustered around the origin of the 2D spectrum. Since the artifact and baseline information spatial frequency content are expected to be fairly well separated (as shown below), the problem is well suited to filtering methods in Fourier space [21]. Fig. 2 illustrates the complete artifact filtering process. Note that, due to the aperiodic nature of the reflectance maps (Fig. 1), their discrete Fourier transforms (DFTs) will exhibit a strong cross shaped pattern centered on the origin. To facilitate the filtering process, the images are first separated into "smooth" and "periodic" components [22]. The smooth component captures most of the aperiodicity edge effects while showing very slow variations else-where, whereas the periodic component contains most of the relevant image information. The filter can then be designed for, and applied to, the periodic component only. The filtered map is obtained by combining the unfiltered smooth component image with the filtered periodic component. Fig. 2(a) shows the DFT of the reflectance map from Fig. 1 (b), while Fig. 2(b) and (c) show the DFTs of its smooth and periodic components, respectively. Note that the cross shaped pattern has been greatly reduced in Fig. 2 (c) compared to Fig. 2(a) by the smooth/-periodic decomposition. Fig. 2(d) shows the DFT of the periodic component of the reflectance map from Fig. 1(a), without the artifact, where the spatial frequency content of the baseline information is concentrated around the origin. A comparison of Fig. 2(c) with Fig. 2(d) reveals that the spatial frequency content due to the artifact is a sym-metric pair of elongated oval-shaped areas, away from the origin, along a diagonal at an angle of $\Theta = \pi/2 + \alpha = \pi/2 - \tan^{-1}(\Delta t/\Delta\lambda)$ from the horizontal, as expected.

For simplicity, the filter is designed as a single elliptically shaped stopband centered on the origin. The orientation of the ellipse (Θ) is determined from the experimental design (spectral bandwidth $\Delta\lambda$ and chirp of the pump Δt) while the size of the ellipse is chosen to cover the two elongated ovals due to the artifact. A passband area centered on the

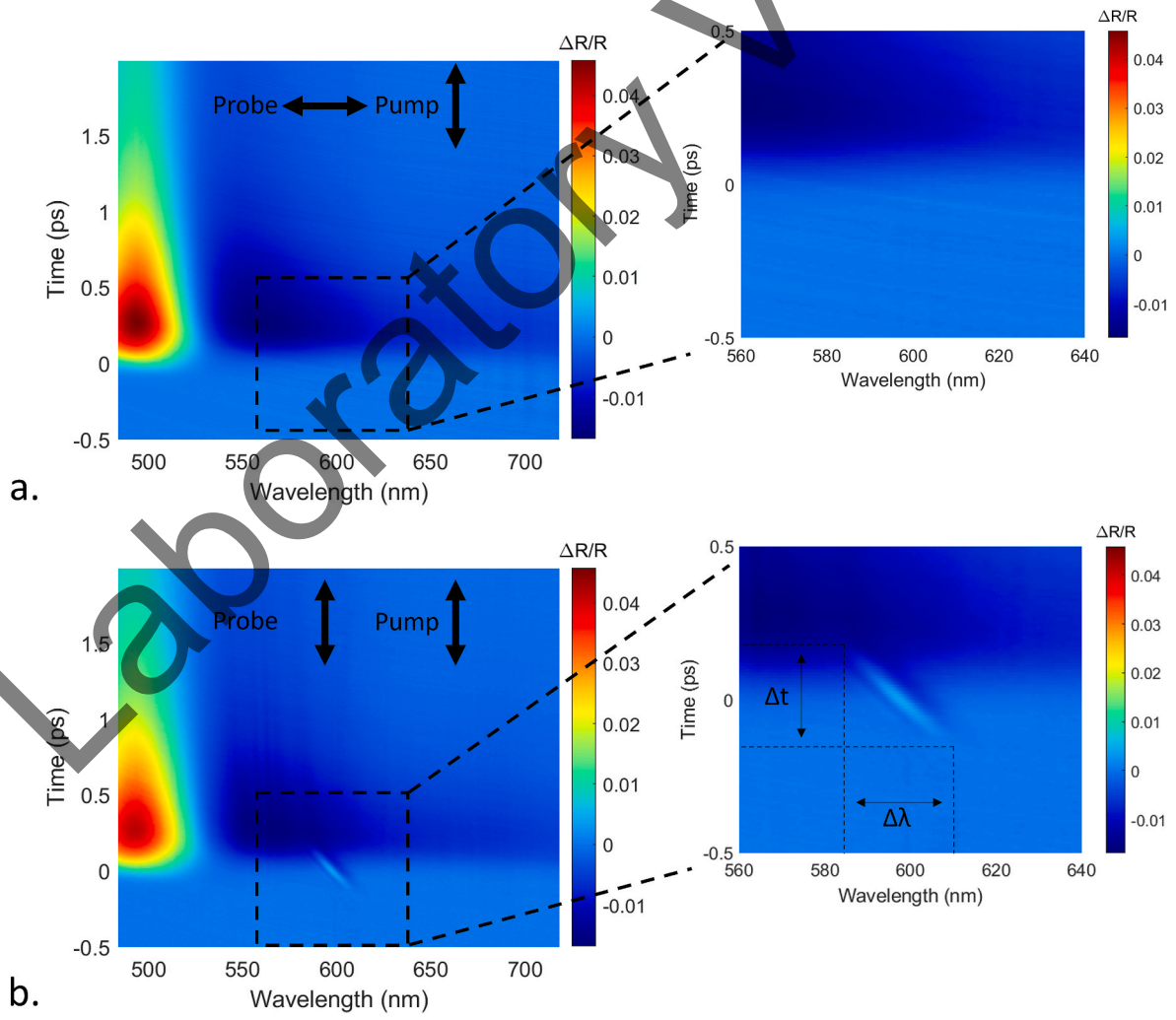

Fig. 1. Transient reflectance maps acquired with (a) mutually perpendicular and (b) mutually parallel pump and probe polarizations. Inserts show portions of the images delimited by the square outlines.

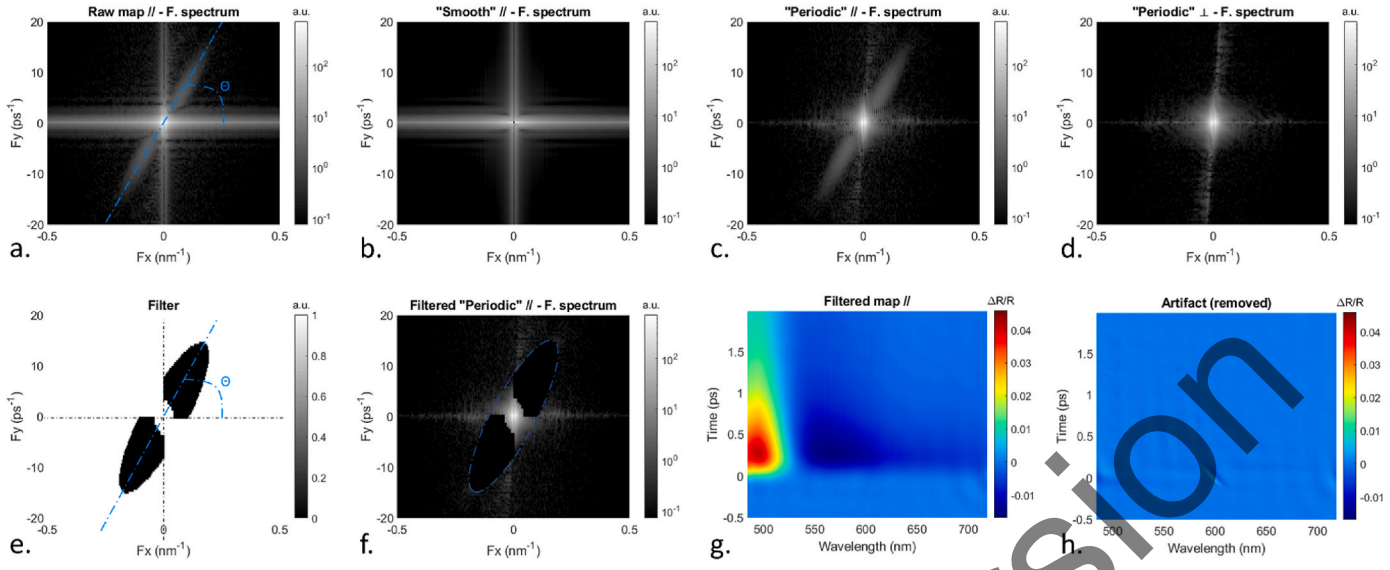

Fig. 2. Filtering process. (a): DFT of the reflectance map from Fig. 1(b); (b) and (c): DFTs of the smooth and periodic components of Fig. 1(b); (d): DFT of the periodic component from Fig. 1(a) without the artifact; (e): Filter binary image, $\Theta = \pi/2 - \tan^{-1}(\Delta t/\Delta\lambda)$; (f): Result of multiplying the filter (e) with the DFT of the periodic component (c); (g): Filtered result following the DFT^{-1} of (f), summation with the smooth component and a light Gaussian blur; (h): application of the inverse filter to isolate the artifact. The "⊥" and "//" symbols in the titles refer to the mutually perpendicular and parallel pump/probe polarization configurations, respectively. Note that only the central portions of the spectra are shown to emphasize the relevant spatial frequency content, the full spectra have size $\pm 50\ ps^{-1} \times \pm 2.2\ nm^{-1}$.

origin preserves the low frequency content of the baseline spectroscopy data. In addition, given that the artifact spatial frequency content is known to be concentrated in the upper-right and lower-left quadrants of the Fourier domain, we found that filtering performance could be improved by adding passbands covering the upper-left and lower-right quadrants (not including the vertical and horizonal axes centered on the origin which are handled by the smooth/periodic decomposition). The resulting filter binary image is shown in Fig. 2(e). Fig. 2(f) shows the result of multiplying the filter by the periodic component DFT in Fig. 2 (c), while Fig. 2(g) shows the final result following a DFT^{-1} of Fig. 2(f), summation with the smooth component, and a light Gaussian blur ($\sigma = 3$) to remove high frequency noise. Fig. 2(f) shows that the artifact has been removed with minimal distortion to the original data. For completeness, Fig. 2(h) shows the results of applying the inverse filter to the original image to isolate the artifact.

The dimensions of the filter ellipse and extent of the central pass-band area are determined automatically by thresholding the DFT of the periodic component in Fig. 2(c). An "upper" threshold is used to delimit the extent of the central pass-band area about the origin, generating a first binary image. A "lower" threshold is used to delimit the pair of elongated oval-shaped areas due to the artifact, generating a second binary image. In both cases, the morphological operations [23] of erosion (3×3) followed by dilation (5×5) are used to de-noise the resulting binary images and consolidate the above-threshold pixel areas. The ellipse dimensions are determined from the second binary image with line searches for above-threshold pixels starting from the origin along the known directions of the long (Θ) and short ($\Theta + \pi/2$) axes of the ellipse. The complete binary filter is then generated from a base image filled with values of one (1.0), drawing the ellipse stop-band (pixel values of 0.0), adding the central passband (setting above-threshold pixels from the first binary image to 1.0), and adding the passbands for the upper-left and lower-right quadrants (setting the quadrant pixels to 1.0). The two thresholds must be finetuned by trial and error to reach the optimal compromise between effectively removing the artifact while preserving the baseline information, though this is normally required only once for a set of experimental conditions. The Python code for the filtering process is publicly available and a link for the code is provided in the supplementary materials.

Fig. 3 compares transient reflectance change profiles at a single wavelength for the data in Figs. 1 and 2 (600 nm, the central wavelength of the pump). The figure shows line profiles for 3 cases: *black curve,* from the raw reference reflectance map in Fig. 1(a), baseline only without artifact; *red curve,* from the raw reflectance map in Fig. 1(b), baseline + artifact; *blue curve*, from the filtered map in Fig. 2(g). The red and blue curves in Fig. 3(b) show the differences from the reference for the raw and filtered profiles from Fig. 3(a), respectively. The standard deviation of the difference between the reference and filtered profiles is 2.9×10^{-4}, indicating a good performance by the filter with minimal distor-tion of the original baseline data. The slight offset between the reference and filtered profiles (-3.5×10^{-4} mean difference) in Fig. 3(a) is likely due to differences in experimental conditions.

3.2. Application to complex samples

To assess the robustness of the proposed artifact removal method, the filter was applied to transient transmittance maps acquired from more complex samples: a nanostructured gold film on a glass substrate and a solution of rhodamine fluorophores in ethanol and CS_2 in a cuvette. The data were acquired with mutually parallel pump and probe polarizations to generate transient grating artifacts. In both cases, measurement with mutually perpendicular pump-probe polarization cannot be used as a reference measurement since both sample responses are polarization dependent. The pump was centered on the optimal resonant/absorption wavelengths in both cases to maximize the presence of the artifacts (675 nm for the nano-cross array, 570 nm for the rhodamine solution). Fig. 4 shows the raw maps, filtered maps, isolated artifacts, and transient transmittance time profiles at maximum artifact presence for the metal nanostructures and rhodamine samples, in the top and bottom rows, respectively. For the nanostructures, the positive time $\Delta T/T$ response centered at 675 nm (top-left map) corresponds to the attenuation and broadening of the surface plasmon resonances [24] in the long arms of the crosses. The top-right graph of Fig. 4 shows the temporal profile at 674 nm, where the artifact causes deviations in the $\Delta T/T$ rising edge around the zero-delay time that would impede the precise estimation of the instrument response function and zero-delay time. For the rhoda-mine solution, the positive time $\Delta T/T$ response centered at 570 nm is due to the bleaching of the fluorophores. The bottom-right graph of Fig. 4 shows the temporal profile at 567 nm, where the artifact significantly

Version of LN2 Laboratoire : 10/2023 Find the manuscript on Analytica Chemica Acta doi.org/10.1016/j.aca.2023.341820

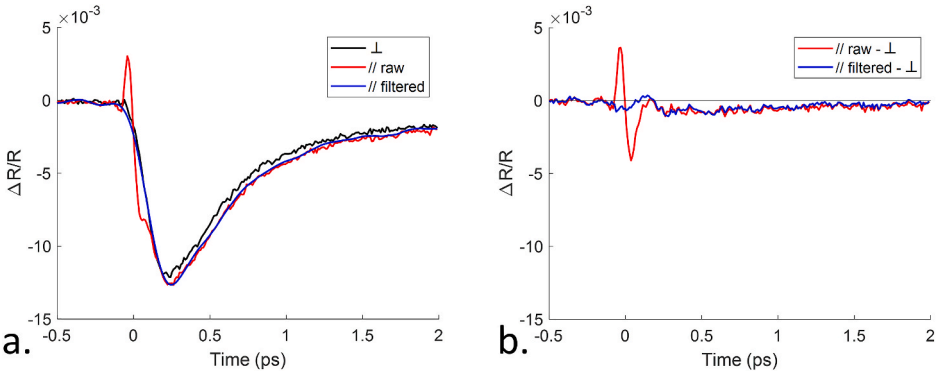

Fig. 3. Transient reflectance profiles at a single wavelength ($\lambda = 600$ nm). (a) Line profiles for 3 cases: *black curve*, from the reference image without artifact in Fig. 1 (a); *red curve*, from the raw image with artifact in Fig. 1(b); *blue curve*, from the filtered map in Fig. 2(g); (b) differences from the reference for the raw and filtered profiles in (a). The standard deviation of the difference between the reference and filtered profiles is 2.9×10^{-4}. The offset between the reference and filtered profiles (-3.5×10^{-4} mean difference) in (a) is likely due to differences in experimental conditions. The "⊥" and "//" symbols in the legends refer to the mutually perpendicular and parallel pump/probe polarization configurations, respectively. (For interpretation of the references to colour in this figure legend, the reader is referred to the Web version of this article.)

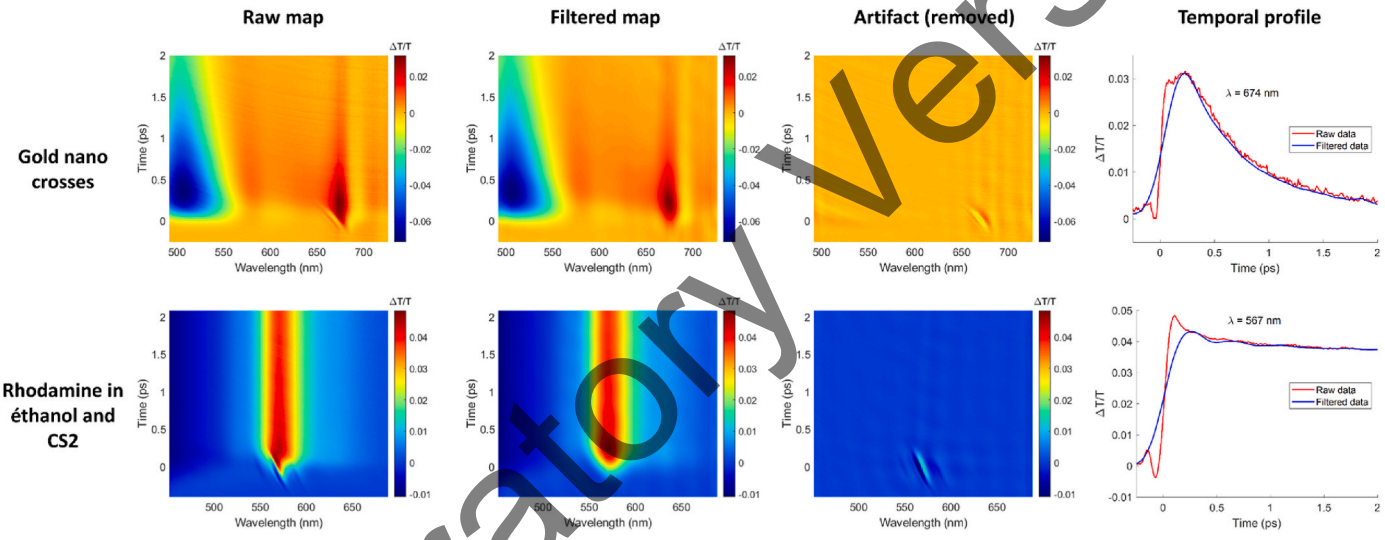

Fig. 4. Raw and filtered transient transmittance maps for two types of complex samples. Top row: metal nanostructures on thin gold film and BK7 substrate; Bottom row: solution of rhodamine in ethanol and CS_2 in a cuvette. The pump was centered on the resonant/absorption wavelengths for both cases to maximize the presence of the artifact (675 nm for the nano-cross array, 570 nm for the rhodamine solution). (For interpretation of the references to colour in this figure legend, the reader is referred to the Web version of this article.)

alters the $\Delta T/T$ dynamics and would lead to an incorrect estimation of the fluorophore characteristic lifetime. In both cases, the filtering successfully removed the distortions by artifact.

4. Conclusion

This paper proposed a 2D method to remove transient grating artifacts from time-resolved spectroscopy data based on filtering in the Fourier domain. The method is simple, intuitive, and requires only forward and backward 2D FFTs. Filtering parameters are determined automatically from the experimental design and semi-automatically from the spectra using two user-supplied thresholds. The effectiveness of the method was demonstrated with transient reflectance maps acquired from a bare gold film with and without transient grating artifacts using mutually parallel and perpendicular pump/probe polarizations. The robustness of the method was demonstrated with transient transmittance maps acquired from more complex samples (nanostructured Au film on a glass substrate and rhodamine fluorophores in solution). As with any problem based on filtering in the Fourier domain, the main limitation of the method is the degree of spectral content overlap between the "information" (the smooth baseline image in this case and the "noise" (the artifact. In cases where the spectral bandwidth and/or chirp of the pump are insufficient, there may be a significant level of spectral overlap and the proposed artifact removal method may have reduced efficacy. The method is expected to be applicable to coherent artifact removal in other types of time and wavelength-resolved spectroscopy data. For example, stimulated Raman artifacts have a shape similar to transient grating artifacts but repeat with a given periodicity in the spectroscopy maps. Since identical shapes that repeat in an image differ only in phase in the Fourier domain, the proposed filtered method should perform well in this circumstance. Indeed, the results shown in Fig. 4 display similar periodicity characteristics for the artifact and the proposed method does performs well.

Funding

This work was supported by the Natural Sciences and Engineering Research Council of Canada (NSERC with Discovery Grants for M. Canva, J-F. Bryche and P.G. Charette. A doctoral scholarship from IDEX Paris-Saclay supports M. Vega. This work is supported by the "ADI"

project funded by the IDEX Paris-Saclay, ANR-11-IDEX-0003-02. LN2 is an International Research Laboratory (IRL) funded and co-operated by Université de Sherbrooke (UdS), Centre National de la Recherche Scientifique (CNRS), Ecole Centrale Lyon (ECL), Institut National des Sciences Appliquées de Lyon (INSA Lyon), and Université Grenoble Alpes (UGA). The work was also financially supported by the Fond de Recherche du Québec Nature et Technologies FRQNT and CMC Microsystems.

CRediT authorship contribution statement

M. Vega: Conceptualization, Software, Formal analysis, Investigation, Writing – original draft, Writing – review & editing. **J.-F. Bryche:** Conceptualization, Investigation, Resources, Writing – review & editing, Supervision, Funding acquisition. **P.-L. Karsenti:** Conceptualization, Investigation, Resources. **P. Gogol:** Software, Writing – review & editing. **M. Canva:** Writing – review & editing, Supervision, Funding acquisition. **P.G. Charette:** Software, Visualization, Writing – review & editing, Supervision, Funding acquisition.

Declaration of competing interest

The authors declare no competing interest.

Data availability

GitHub link to the code and the data used in the article is provided in the following link: https://github.com/laboratoiredebiophotonique/transient_grating_artifact_filter.

Acknowledgement

The authors wish to thank Guillaume Beaudin for his help with the coding.

References

[1] H.J. Eichler, D. Langhans, F. Massmann, Coherence peaks in picosecond sampling experiments, Opt Commun. 50 (2) (1984 May) 117–122.
[2] C. Ruckebusch, M. Sliwa, P. Pernot, A. de Juan, R. Tauler, Comprehensive data analysis of femtosecond transient absorption spectra: a review, J. Photochem. Photobiol. C Photochem. Rev. 13 (1) (2012 Mar) 1–27.
[3] A. Penzkofer, W. Falkenstein, W. Kaiser, Vibronic relaxation in the S1 state of rhodamine dye solutions, Chem. Phys. Lett. 44 (1) (1976) 82–87.
[4] D.F. Underwood, T. Kippeny, S.J. Rosenthal, Ultrafast carrier dynamics in CdSe nanocrystals determined by femtosecond fluorescence upconversion spectroscopy, J. Phys. Chem. B 105 (2) (2001 Jan 1) 436–443.
[5] C.K. Sun, F. Vallée, L.H. Acioli, E.P. Ippen, J.G. Fujimoto, Femtosecond-tunable measurement of electron thermalization in gold, Phys. Rev. B 50 (20) (1994 Nov 15) 15337–15348.
[6] M. Lorenc, M. Ziolek, R. Naskrecki, J. Karolczak, J. Kubicki, A. Maciejewski, Artifacts in femtosecond transient absorption spectroscopy, Appl. Phys. B Laser Opt. 74 (1) (2002 Jan 1) 19–27.
[7] C.W. Luo, Y.T. Wang, F.W. Chen, H.C. Shih, T. Kobayashi, Eliminate coherence spike in reflection-type pump-probe measurements, Opt Express 17 (14) (2009 Jul 6), 11321.
[8] Z. Vardeny, J. Tauc, Picosecond coherence coupling in the pump and probe technique, Opt Commun. 39 (6) (1981 Nov) 396–400.
[9] S.A. Kovalenko, A.L. Dobryakov, J. Ruthmann, N.P. Ernsting, Femtosecond spectroscopy of condensed phases with chirped supercontinuum probing, Phys. Rev. 59 (3) (1999 Mar 1) 2369–2384.
[10] A. Lapini, S.M. Vázquez, P.T. Touceda, M. Lima, Cross-phase modulation in visible-pump/mid-infrared-probe spectroscopy, J. Mol. Struct. 993 (1–3) (2011 May) 470–473.
[11] K.F. Lee, P. Nuernberger, A. Bonvalet, M. Joffre, Removing cross-phase modulation from midinfrared chirped-pulse upconversion spectra, Opt Express 17 (21) (2009 Oct 12), 18738.
[12] H.J. Eichler, P. Günter, D.W. Pohl [cited 2022 Nov 28]. (Tamir T, editor. Springer Series in Optical Sciences, in: Laser-Induced Dynamic Gratings [Internet], vol. 50, Springer Berlin Heidelberg, Berlin, Heidelberg, 1986. Available from: http://link.springer.com/10.1007/978-3-540-39662-8.
[13] H. Liu, H. Zhang, J.H. Si, L.H. Yan, F. Chen, X. Hou, Elimination of the coherent artifact in a pump-probe experiment by directly detecting the background-free diffraction signal, Chin. Phys. Lett. 28 (8) (2011 Aug), 086602.
[14] S.L. Palfrey, T.F. Heinz, Coherent interactions in pump–probe absorption measurements: the effect of phase gratings, J. Opt. Soc. Am. B 2 (4) (1985 Apr 1) 674.
[15] T.F. Heinz, K.B. Eisenthal, S.L. Palfrey, Coherent coupling effects in pump–probe measurements with collinear, copropagating beams, Opt Lett. 9 (8) (1984 Aug 1) 359.
[16] R.A. Engh, J.W. Petrich, G.R. Fleming, Removal of coherent coupling artifact in ground-state recovery experiments: malachite green in water-methanol mixtures, J. Phys. Chem. 89 (4) (1985 Feb) 618–621.
[17] O. Devos, N. Mouton, M. Sliwa, C. Ruckebusch, Baseline correction methods to deal with artifacts in femtosecond transient absorption spectroscopy, Anal. Chim. Acta 705 (1–2) (2011 Oct) 64–71.
[18] J.J. de Rooi, O. Devos, M. Sliwa, C. Ruckebusch, P.H.C. Eilers, Mixture models for two-dimensional baseline correction, applied to artifact elimination in time-resolved spectroscopy, Anal. Chim. Acta 771 (2013 Apr) 7–13.
[19] J.F. Bryche, M. Vega, J. Moreau, P.L. Karsenti, P. Bresson, M. Besbes, et al., Ultrafast heat transfer at the nanoscale: controlling heat anisotropy, ACS Photon. 10 (4) (2023) 1177–1186.
[20] Y. Wang, H. Shi, L. Shen, Y. Wang, S.B. Cronin, J.M. Dawlaty, Ultrafast dynamics of hot electrons in nanostructures: distinguishing the influence on interband and plasmon resonances, ACS Photonics 6 (9) (2019 Sep 18) 2295–2302.
[21] R. Gonzalez, R. Woods, Digital Image Processing, fourth ed., Pearson, New York, NY, 2017, p. 1192.
[22] L. Moisan, Periodic plus smooth image decomposition, J. Math. Imag. Vis. 39 (2) (2011 Feb) 161–179.
[23] R.C. Gonzalez, R.E. Woods, Digital Image Processing, Pearson, New York, NY, 2018, p. 1168.
[24] S. Link, C. Burda, Z.L. Wang, M.A. El-Sayed, Electron dynamics in gold and gold–silver alloy nanoparticles: the influence of a nonequilibrium electron distribution and the size dependence of the electron–phonon relaxation, J. Chem. Phys. 111 (3) (1999 Jul 15) 1255–1264.